NASA Technical Memorandum 110282

A Comparison of Pressure Measurements Between a Full-Scale and a 1/6-Scale F/A-18 Twin Tail During Buffet

Robert W. Moses
Langley Research Center, Hampton, Virginia

Ed Pendleton
Wright Laboratory, Wright Patterson Air Force Base, Ohio

August 1996

National Aeronautics and
Space Administration
Langley Research Center
Hampton, Virginia 23681-0001

A COMPARISON OF PRESSURE MEASUREMENTS BETWEEN A FULL-SCALE AND A 1/6-SCALE F/A-18 TWIN TAIL DURING BUFFET

Robert W. Moses*

Ed Pendleton**

SUMMARY

In 1993, tail buffet tests were performed on a full-scale, production model F/A-18 in the 80-by-120 Foot Wind Tunnel at NASA Ames Research Center. Steady and unsteady pressures were recorded on both sides of the starboard vertical tail for an angle of attack range of 20 to 40 degrees and at a sideslip range of -16 to 16 degrees at freestream velocities up to 100 knots (Mach 0.15, Reynolds number $1.23*10^7$). The aircraft was equipped with removable leading edge extension (LEX) fences that are used in flight to reduce tail buffet loads.

In 1995, tail buffet tests were performed on a 1/6-scale F-18 A/B model in the Transonic Dynamics Tunnel (TDT) at NASA Langley Research Center. Steady and unsteady pressures were recorded on both sides of both vertical tails for an angle-of-attack range of 7 to 37 degrees at freestream velocities up to 65 knots (Mach 0.10).

Comparisons of steady and unsteady pressures and root bending moments are presented for these wind-tunnel models for selected test cases. Representative pressure and root bending moment power spectra are also discussed, as are selected pressure cross-spectral densities.

LIST OF SYMBOLS

A_j	area of j-th tail element (ft^2)
A_F	total planform area of tail (ft^2)
C_{M_B}	tail root bending moment coefficient
$C_{\Delta p}$	differential pressure coefficient
$\bar{c}$	wing mean aerodynamic chord (ft)
F(n)	nondimensional buffet pressure power spectral density function
f	frequency (Hz)
M	Mach number
n	frequency parameter, $f\bar{c}/U_\infty$
$p_{in(out)}$	pressure on inner (outer) tail surface (psi)
Δp	differential pressure, p_{in} - p_{out} (psi)
q_∞	freestream dynamic pressure (psi)
t	time (sec)
U_∞	freestream velocity (ft/s)
$\bar{y}_j$	distance from root of tail to centroid of j-th tail area element (ft)
α	angle of attack (degrees)
$\overline{(\ )}$	indicates steady (mean) value
$(\ )'$	indicates root-mean-square value
$(\ )''$	indicates power spectral density

1. INTRODUCTION

Buffet is a primary cause of structural fatigue of tails in many twin-tail fighter aircraft. The F/A-18, in particular, experienced fatigue problems due to tail buffet caused by breakdown of the vortices shed from the leading edge extensions (LEXs) at high angles-of-attack[1,2]. The severity of this problem was reduced by installing a trapezoidal vertical plate, which is known as the LEX fence, on each LEX just forward of the wing-fuselage junction[1,2]. Interaction of the LEX vortices with the LEX fence alters the characteristics of the unsteady forces imposed on the vertical tails, thereby reducing the severity of the buffeting response[1,2].

The results of full-scale wind-tunnel tests, designed to quantify the pressure field that exists on the F/A-18 starboard tail in a buffet environment at various angles of attack and sideslip, are shown here. The resulting root bending moment coefficients are also illustrated. F/A-18 tail buffet has been studied intensively in both the experimental[1-9] and computational arenas[10,11], but the full-scale tests described herein present a unique opportunity to explore several aspects of the tail buffet phenomenon without the model geometric scaling constraints present in most reduced-scale wind-tunnel studies.

The principal objectives of the full-scale tests were: (1) to quantify the steady and unsteady pressures that exist on the vertical tail in a buffet flow environment over a wide range of angle of attack and sideslip conditions, (2) to further quantify the effects of the LEX fence in reducing tail buffet, and (3) to provide detailed data for comparison with reduced-scale wind tunnel and computational results available from other sources[12].

The results of the 1/6-scale wind-tunnel tests, designed to quantify the pressure field that exists on the F/A-18 starboard tail in a buffet environment at various angles-of-attack, are described herein.

The primary objectives of the 1/6-scale tests were: (1) to determine the effectiveness of the rudder, of piezoelectric actuators, and of other aerodynamic devices in alleviating buffeting, (2) to quantify the phasing of the differential

* Program Manager, 1/6-Scale Study known as Actively Controlled Response Of Buffet Affected Tails (ACROBAT), Aeroelasticity Branch, MS 340, NASA Langley Research Center, Hampton, VA 23681-0001

** Program Manager, Full-Scale Study, Wright Laboratory, Wright-Patterson Air Force Base, Ohio 45433

unsteady pressures that exist on the vertical tail in a buffet flow environment over a wide range of angle of attack, (3) to further quantify the propogation speed of the unsteady pressure as it moved down the tail, and (4) to provide detailed data for comparison with full-scale data from other sources[12].

The purpose of this paper is to highlight the similarities and differences between the full-scale and 1/6-scale wind-tunnel data by comparing power spectra, cross spectra, and scaling relationships. Of primary interest is the phase reported in the cross spectral densities for differential pressures between leading-edge and trailing-edge stations.

2. EXPERIMENTAL SETUPS

2.1 80x120 Wind Tunnel and Full-Scale Test Article

The test article, supplied by the US Navy, was from the first F/A-18 model A production block. The engines and avionics were removed prior to shipment to the wind tunnel. For these studies, the test article was configured with flow-through inlets and the missile rails were left in place. The test article, installed in the 80- by 120-Foot Wind Tunnel at the NASA Ames Research Center, is shown in Figure 1.

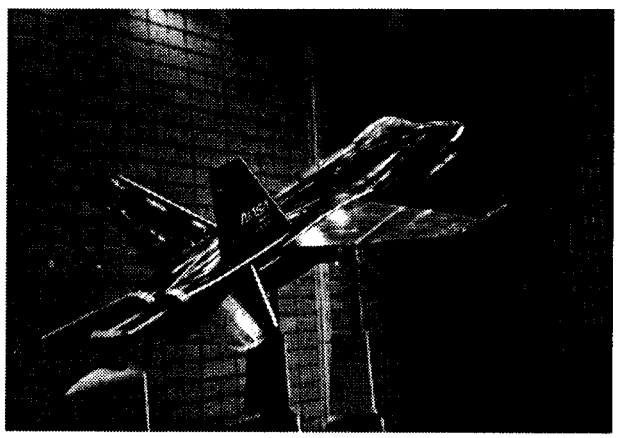

Figure 1. The F/A-18 in the 80'x120' Wind Tunnel at the NASA Ames Research Center

Geometric dimensions of the F/A-18 aircraft are: overall length (56.0 ft), wing span (37.42 ft), wing reference area (400 ft^2), wing mean aerodynamic chord (11.52 ft), and vertical tail reference area (52.12 ft^2). The leading-edge flaps were fixed at a deflection angle of 34 degrees down and the trailing-edge control surfaces were fixed at a zero deflection angle for all runs. These control surface settings are representative of the standard control-law scheduled deflections for angles-of-attack greater than 26 degrees. The rudders were fixed in their zero deflection position throughout the test envelope, and the horizontal stabilators were actuated to match the orientation of those on the High Angle-of-Attack Research Vehicle (HARV) for steady, trimmed flight at each angle of attack.

Pressures and tip accelerations were measured on the starboard vertical tail surfaces of the F/A-18 full-scale model.

2.2 TDT and 1/6-Scale Test Article

The test article was a 1/6-scale F-18 A/B drop model that was outfitted with interchangeable rigid and flexible vertical tails on both sides. The starboard vertical tails were configured with an active rudder for performing buffeting alleviation studies.

Likewise, the deflection angles of the leading-edge flaps, trailing edge flaps, rudder (when not actuated), and the horizontal stabilators were set identically to the F/A-18 aircraft as listed above.

Pressures, root strain, and tip accelerations were measured on the starboard and port vertical tail surfaces. The test article, installed in the TDT at the NASA Langley Research Center, is shown in Figure 2.

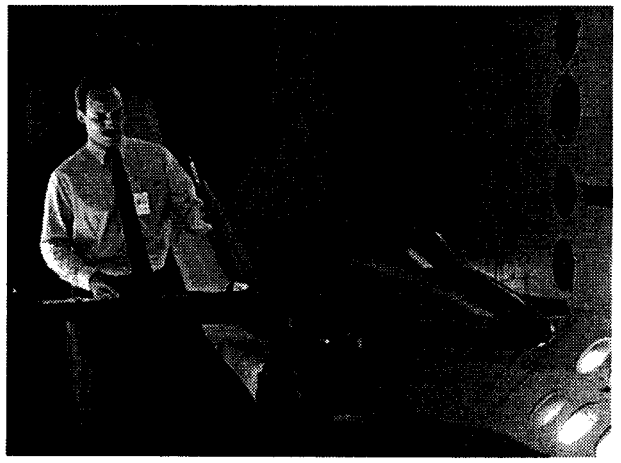

Figure 2. The 1/6-Scale F/A-18 model in the Transonic Dynamics Tunnel at the NASA Langley Research Center

2.3 Ground Vibration Test of Full-Scale Tails

A ground vibration test (GVT) was conducted in preparation for the full-scale tests to determine the modes and natural frequencies of the tail structure when the full-scale model was mounted on the wind-tunnel struts. Table 1 lists the resulting symmetric (S) and anti-symmetric (A) modes and natural frequencies of the vertical tails. Levraera et al[13] give further information on the dynamic characteristics of the vertical tails, including mode shapes.

Table 1. Full-Scale Vertical Tail Modes

Mode	Frequency (Hz)
1st bending (S, A)	15.4, 15.3
1st torsion (S, A)	44.2, 45.4
2nd bending (S, A)	61.3, 61.9

2.4 Ground Vibration Test of 1/6-Scale Tail

A GVT was conducted on the 1/6-scale model to determine the modes and natural frequencies of the tail structure when the 1/6-scale model was sting-mounted in the TDT. Table 2 lists resulting natural frequencies for the modes of the flexible tails.

During the GVT, a rigid vertical tail was mounted on the port side, opposite the flexible tail on the starboard side. The modes reported in Table 2 are for the starboard tail only.

Table 2. 1/6-Scale Vertical Tail Modes

Mode	Frequency (Hz)
1st bending	16.5
1st torsion	58.5
2nd bending	71.5

2.5 Instrumentation on Full-Scale Model

Seventy-two Kulite pressure transducers (model LQ-167-125-10SG) were mounted on the starboard vertical tail of the F/A-18 prior to installation of the test article in the wind tunnel. These sensors were located in a 6-by-6 grid on either side of the tail as illustrated in Figure 3.

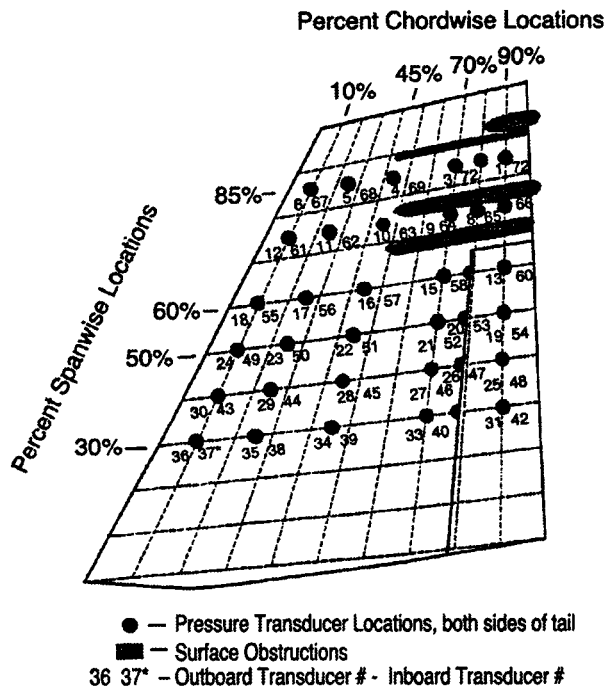

Figure 3. Pressure Transducer Locations on Full-Scale Starboard Vertical Tail

2.6 Test Procedure for Full-Scale Model

Steady and unsteady data were acquired for approximately 30 seconds at each test condition. Each channel was sampled simultaneously at a rate of 3.32 samples per sampling cycle. Each of the signals passed through an anti-aliasing, 6 pole butterworth filter with a nominal cut-off frequency of 500 Hz prior to digitization. The transducer signals then passed through one of five Aydin-Vector pulse code modulation (PCM) multiplexers (model SCU-700-16), which digitized the signals prior to their being recorded on magnetic tape.

2.7 Instrumentation on 1/6-Scale Model

Twenty-eight, thirty, and thirty Kulite pressure transducers (model LQ-167-125-10SG) were mounted on the starboard flexible vertical tail, starboard rigid vertical tail, and port rigid vertical tail, respectively, of the 1/6-scale F/A-18 model prior to installation of the test article in the wind tunnel. These sensors were located in the pattern on either side of the tail as illustrated in Figures 4 and 5 for the starboard flexible and starboard rigid tails, respectively. The pattern on the starboard flexible tail was chosen for investigating pressures created by the responses of the flexible tails to buffet. Therefore, the transducers are concentrated toward the tip of the tail.

The flexible tails' response to buffet was measured using a full-bridge strain gage at the root and two tip accelerometers (leading edge and trailing edge).

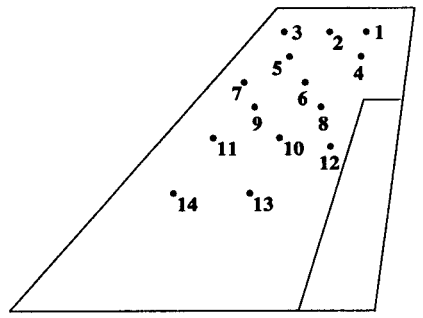

Figure 4. Pressure Transducer Locations on 1/6-Scale Starboard Flexible Vertical Tail

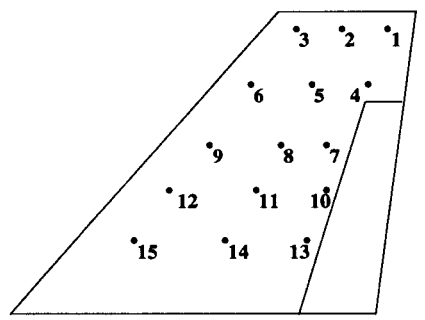

Figure 5. Pressure Transducer Locations on 1/6-Scale Starboard Rigid Vertical Tail

2.8 Test Procedure for 1/6-Scale Model

Steady and unsteady data were acquired for approximately 30 seconds at each test condition. Each channel was sampled simultaneously at a rate of 3.27 samples per sampling cycle. Each of the signals passed through an anti-aliasing, 6 pole butterworth filter with a nominal cut-off frequency of 2000 Hz prior to digitization. The transducer signals then passed through one of three Aydin-Vector pulse code modulation (PCM) multiplexers

(model SCU-700-16), which digitized the signals prior to their being recorded on magnetic tape.

This system is the same system used in the full-scale test except that a faster sampling rate was used. To resolve the propogation speed of the unsteady pressure wave as it moves past the vertical tail, a sampling rate higher than 500 Hz was necessary. Therefore, the only alternative sampling rate for the system, 2000 Hz, was chosen. Thus, time domain analysis in addition to frequency domain analysis could be used in characterizing the flowfield during buffet.

2.9 Full-Scale Test Conditions

A wind-off, baseline run was performed to record the null levels of the pressure transducer signals before the buffet tests were initiated.

Fifty-nine runs were conducted at a freestream velocity of 168 ft/s, which corresponded to a dynamic pressure of 33 psf , a Mach number of 0.15, and a Reynolds number of $1.23*10^7$ based on the mean aerodynamic chord. The four remaining runs were conducted at a freestream velocity of 102 ft/s and a dynamic pressure of 20 psf. Angle of attack was varied from 20 to 40 degrees for all runs.

2.10 1/6-Scale Test Conditions

Over sixty runs were completed during two TDT entries at various angles-of-attack without a LEX fence. Prior to and after each run, wind-off, baseline pressure signals were acquired to record the null levels of the transducers.

Most of the runs were conducted in atmospheric air at a freestream velocity of 110 ft/s, which corresponds to a dynamic pressure of 14 psf, and a Mach number of 0.10. This condition was chosen by scaling, using the Strouhal number, a full-scale condition of 340 psf at which severe buffeting occurs[11].

3. Data Reduction

3.1 Full-Scale Model

Reduction of the pressure transducer signals initially involved subtracting the pressure values obtained during the baseline run from each of the subsequent pressure signals. This process ensured that all pressures were measured relative to the proper zero reference levels since the microphones could not be nulled in the tunnel.

Steady pressure differences at each transducer-pair station were computed by subtracting the mean of the outer surface transducer signal from the mean of the inner surface transducer signal. The unsteady, or buffet, pressures were assumed to be zero-mean, stationary random processes amenable to standard analysis techniques in the time and frequency domains. Differential pressure time histories were computed at each transducer-pair station for each test condition by subtracting the outer surface pressure reading from the inner surface pressure reading at each time step.

The differential pressure and acceleration time histories were converted to the frequency domain using Fast Fourier Transform (FFT) techniques. Approximately 15 seconds of data from each test condition were divided into blocks, each containing 2048 samples. A Hanning window was applied to reduce bandwidth leakage, and an average of 22 transforms with 50% overlap was used to increase statistical confidence. The resulting frequency resolution was 0.8 Hz. Power spectral density (PSD) functions were computed from the Fourier transforms. Root-mean-square (RMS) values of unsteady pressures and accelerations were then computed from the PSDs via numerical integration.

The dimensionless form chosen for presenting the buffet pressure spectra normalized by the freestream dynamic pressure is suggested by Mabey[14]:

$$\left(p'/q_\infty\right)^2 = \int_{n=0}^{n=\infty} F(n)dn = \int_{\ln(n)=-\infty}^{\ln(n)=+\infty} nF(n)d(\ln n) \quad (1)$$

where F(n) is the nondimensional buffet excitation power spectral density in terms of the frequency parameter, n. The resulting fluctuations of the pressures, normal force, and bending moment are plotted as $\sqrt{nF(n)}$ vs n from n=0 to 8. For q_∞ =33 psf and $\bar{c}$ =11.54 ft, n = 1 corresponds to a dimensional frequency of 14.56 Hz.

3.2 1/6-Scale Model

The unsteady, or buffet, pressures were assumed to be zero-mean, stationary random processes amenable to standard analysis techniques in the time and frequency domains. Differential pressure time histories were computed at each transducer-pair station for each test condition by subtracting the outer surface pressure reading from the inner surface pressure reading at each time step.

The differential pressure and root strain time histories were converted to the frequency domain using Fast Fourier Transform (FFT) techniques. Approximately 16 seconds of data from each test condition were divided into blocks, each containing 8192 samples. A rectangular window was applied to reduce bandwidth leakage, and an average of 9 transforms with 75% overlap was used to increase statistical confidence. The resulting frequency resolution was 0.2 Hz. Power spectral density (PSD) functions were computed from the Fourier transforms.

The dimensionless form chosen for presenting the buffet pressure spectra normalized by the freestream dynamic pressure is:

$$F(n) = P(f) / q_\infty^2 \cdot (U_\infty / \bar{c}) \quad (2)$$

where P(f) is the power spectral density of the pressure. The resulting fluctuations of the pressures are plotted as $\sqrt{nF(n)}$ vs n from n=0 to 5 for a q_∞ =14 psf and $\bar{c}$ =1.92 ft.

4. Results and Discussions

4.1 Full-Scale Model Root-Mean-Square Tail Buffet Loads

Time histories of the unsteady root bending moment coefficient were calculated from the unsteady differential pressures using:

$$C_{\overline{M_B}}(t) = \frac{1}{q_\infty A_F \overline{c}} \sum_{j=1}^{36} \Delta p_j(t) A_j \overline{y}_j \qquad (3)$$

where $\Delta p_j(t) = [p_{in}(t) - p_{out}(t)]_j$ is the differential pressure time history at the j-th transducer-pair station, A_j is the area element around the transducer, and $\overline{y}_j$ is the distance from the root to the centroid of the area element. The corresponding root-mean-square values of the unsteady bending moment coefficients are denoted symbolically by C'_{M_B}.

Figure 6 shows the variation of the RMS value of bending moment coefficient with angle of attack at zero sideslip. The LEX fence produced a considerable decrease in C'_{M_B} from 20 to 36 degrees angle of attack, but the fence-on and fence-off curves converge at an angle of attack of 40 degrees.

Dynamic pressure scale effects are also depicted in Figure 6, where results at 26 and 28 degrees angle of attack for a freestream dynamic pressure of 20 psf are overlaid on the results for 33 psf. For these two angles of attack, this result supports previous findings that the RMS values of the buffet pressures that were used to calculate the time histories of the root bending moment are linear functions of the dynamic pressure in the freestream.[3]

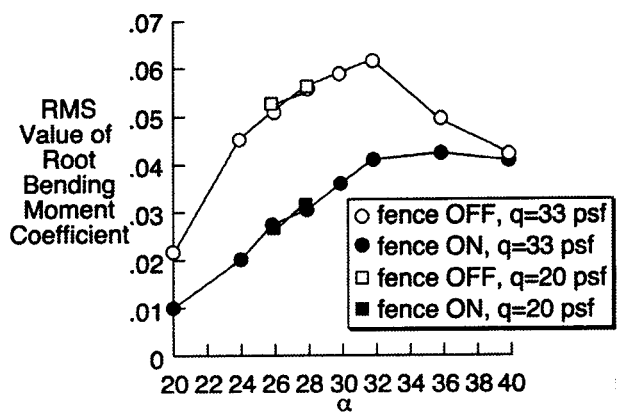

Figure 6. RMS Value of Root Bending Moment Coefficient vs. Angle of Attack in Degrees

4.2 1/6-Scale Model Root-Mean-Square Tail Buffet Loads

The buffet loads on the 1/6-scale vertical tail were obtained more directly by computing the root-mean-square of the time history for the strain gage located at the root of the flexible tail.

Figure 7 shows the variation of the RMS root strain with angle of attack for a dynamic pressure of 14 psf. As shown in Figure 7, the peak buffeting occurs around 36 degrees angle of attack. Several factors could contribute to the peak occurring at 36 degrees rather than 32 degrees angle of attack which was the case for the full-scale model. These factors may include participation of other modes, angle-of-attack calibration for the sting in the TDT prior to the test, or a slightly different vortex trajectory off the LEX. To isolate the factors due to other modes of the model, the PSD of root strain at the frequency of the first bending mode was computed. Presented as normalized values in Figure 8, the PSDs indicated that the maximum response in the first bending mode occurred around 34 degrees angle of attack.

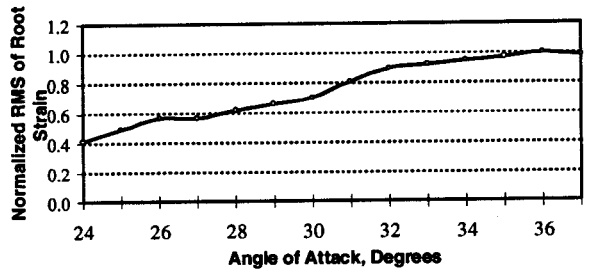

Figure 7. Normalized RMS of Root Strain on 1/6-Scale Vertical Tail

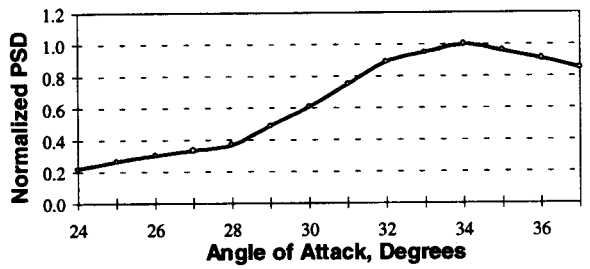

Figure 8. Normalized PSD of Root Strain (at Frequency of First Bending Mode) on 1/6-Scale Vertical Tail

4.3 Full-Scale Model Buffet Pressures-Excitation Spectra

Figure 9(a) and 9(b) present spectra, RMS form, for the transducer-pair station located at 45% chord and 60% span, at two angles of attack. Both LEX fence-off and fence-on results are presented for comparison. At $\alpha = 20^\circ$ in Figure 9(a), the peak of the curve for fence off is rather broad and centered about n=0.9; however, the peak is considerably sharper at $\alpha = 32^\circ$ and centered at n=0.6 in Figure 9(b).

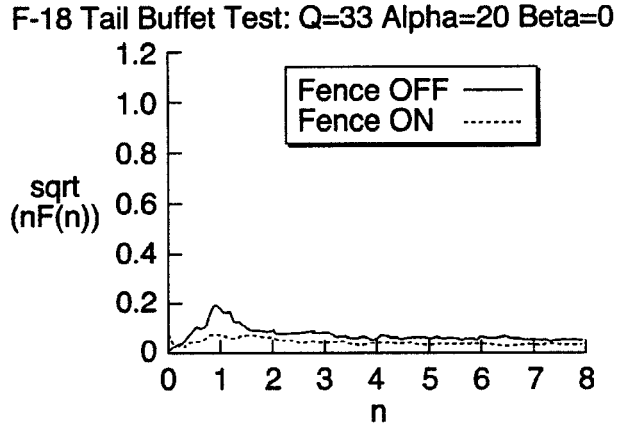

Figure 9(a). Excitation Spectra of Pressures on Full-Scale Tail, $\alpha = 20^\circ$, q = 33 psf

This concentrating of the buffet energy into a narrow frequency band with a higher peak as angle of attack is increased (up to the occurrence of maximum buffet) is typical for the F/A-18. This trend is also noted elsewhere.[1,3]

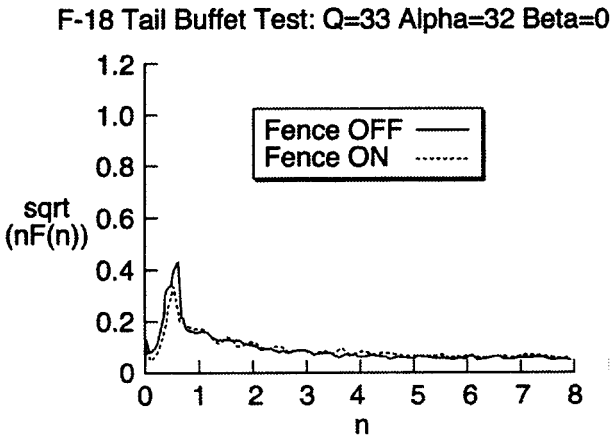

Figure 9(b). Excitation Spectra of Pressures On Full-Scale Tail, $\alpha = 32^\circ$, q = 33 psf

4.4 1/6-Scale Tail Buffet Pressures - Excitation Spectra

Figure 10(a) and 10(b) present spectra, RMS form, for the transducer-pair station located at 50% chord and 60% span, at two angles of attack. There is no LEX fence on the 1/6-scale model. At $\alpha = 20^\circ$ in Figure 10(a), the peak of the curve is rather broad and centered about n=1.2; however, the peak is considerably sharper at $\alpha = 32^\circ$ and centered about n=0.5 in Figure 10(b). Like the F/A-18, this concentrating of the buffet energy into a narrow frequency band with a higher peak as angle of attack is increased (up to the occurrence of maximum buffet) is typical for the 1/6-scale model.

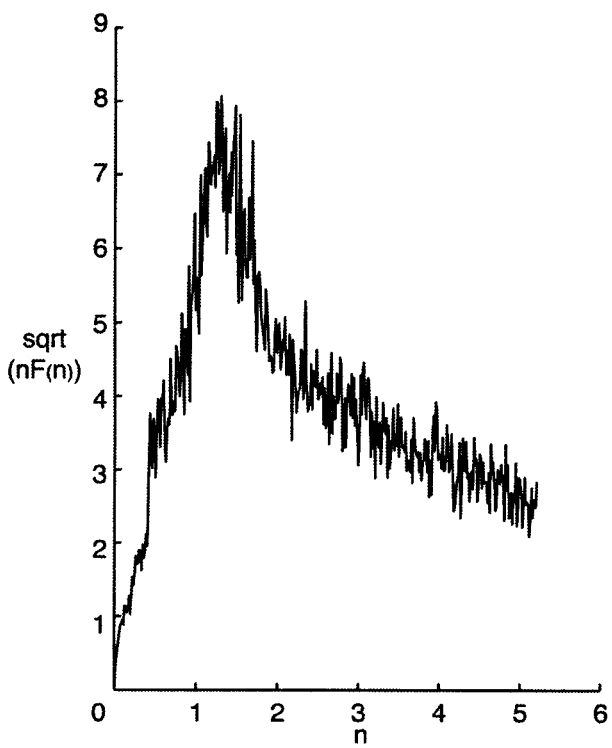

Figure 10(a). Excitation Spectra of Differential Pressures on 1/6-Scale Flexible Tail, $\alpha = 20^\circ$

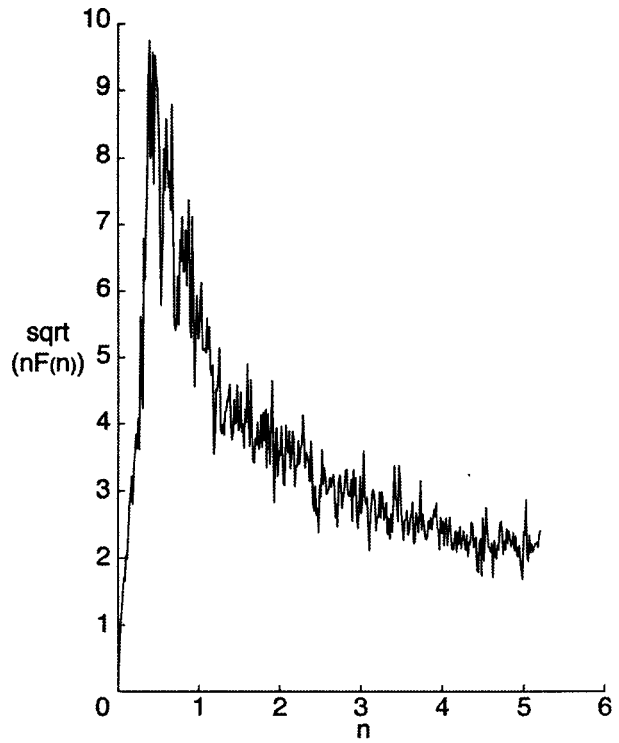

Figure 10(b). Excitation Spectra of Differential Pressures on 1/6-Scale Flexible Tail, $\alpha = 32^\circ$

4.5 Full-Scale Tail Buffet Loads-Power Spectral Densities

Power spectral densities of the root bending moment coefficients were determined from the time histories defined by Equation (3) for each test condition. Representative bending moment coefficient PSDs are presented in Figure 11. Normally, these PSDs would have dimensions of Hz^{-1} since C_{M_B} is dimensionless. Here, the normal force and bending moment coefficient PSDs have been made dimensionless through multiplication by $U_\infty / \bar{c}$.

Figure 11 depicts the root bending moment coefficient power spectral densities, C''_{M_B}, for angles of attack of 20 and 32 degrees. As depicted in Figure 11, the frequency at which the peak bending moment was exerted on the tail decreased with angle of attack. This trend corresponds to the frequency shift with angle of attack discussed previously for the buffet pressures.

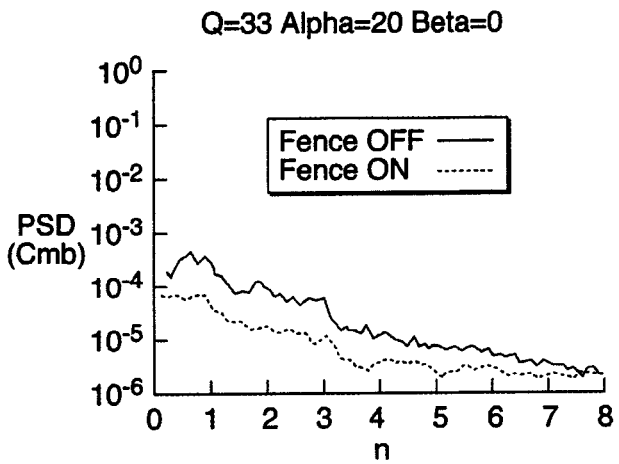

Figure 11(a). PSD of Full-Scale Root Bending Moment Coefficient, $\alpha = 20^\circ$, q=33 psf

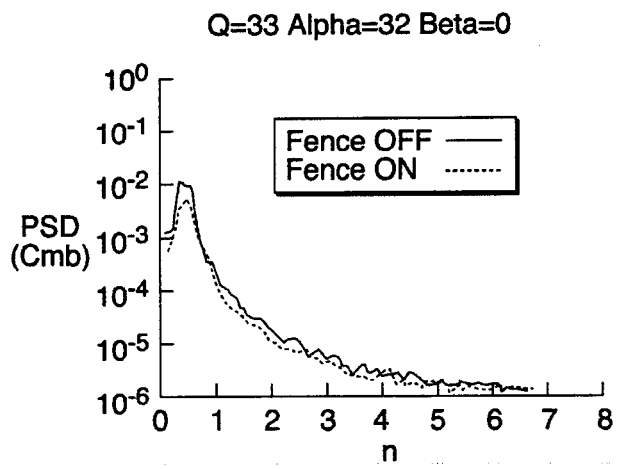

Figure 11(b). PSD of Full-Scale Root Bending Moment Coefficient, $\alpha = 32^\circ$, q=33 psf

4.6 1/6-Scale Model Buffet Loads-Power Spectral Densities

Power spectral densities of the tail root bending moment were computed from the time histories of the root strain gage. PSDs of the tail root bending moment for $\alpha = 20^\circ$ and $\alpha = 32^\circ$ are presented in Figure 12.

In Figure 12, the peak value and the value at 58 Hz correspond to the first bending mode and first torsion mode of the tail, respectively. The response in the first bending mode has grown with the increase in angle of attack while the response in the first torsion mode has diminished slightly. This trend is related to the frequency shift of the excitation spectra with increased angle of attack illustrated in Figure 10.

In both the full-scale test and the 1/6-scale test, the maximum value of the PSD (corresponding to first bending) grows by at least one order of magnitude at $\alpha = 32^\circ$ from its original value at $\alpha = 20^\circ$.

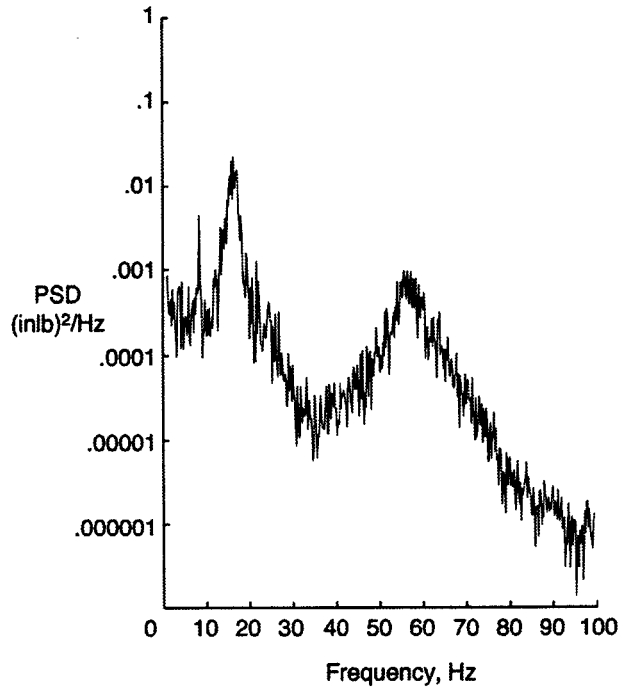

Figure 12(a). PSD of Tail Root Bending Moment, 1/6-Scale Model, $\alpha = 20^\circ$, q=14 psf

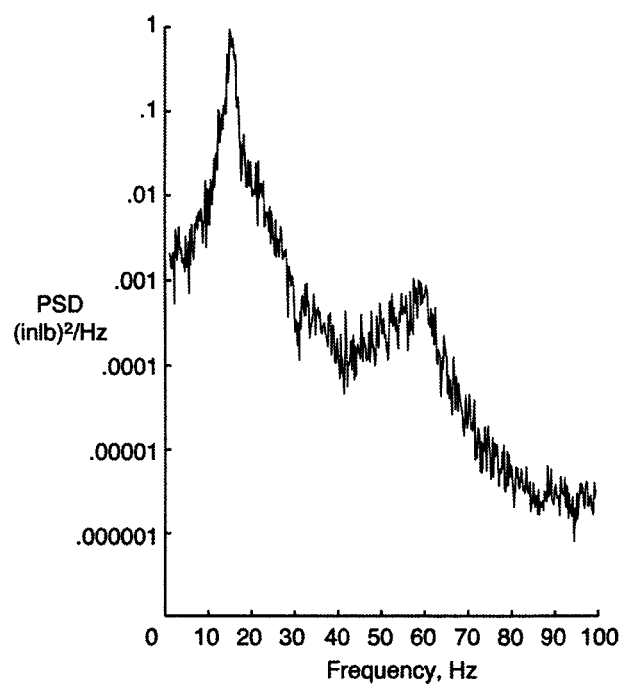

Figure 12(b). PSD of Tail Root Bending Moment, 1/6-Scale Model, $\alpha = 32^\circ$, q=14 psf

4.7 Full-Scale Model Buffet Pressures-Cross Spectral Densities

Further insight into the tail buffet process was gained by computing cross spectral densities (CSDs) between the unsteady pressures acting on the inboard and outboard surfaces at selected locations on the tail. For a given transducer station j, CSD[$(p_{in},p_{out})_j$] was computed for both the LEX fence-off and -on test conditions at angles of attack of 20 and 32 degrees with zero sideslip. These CSDs are presented as coherence and phase angle functions, which are dimensionless. No effort was made to account for any artificial coherence in the pressures due to any response of the tail to the buffet.

CSDs of the unsteady pressure signals from transducer stations near the tip of the tail and along its leading edge generally displayed the strongest levels of buffet excitation. The coherence, magnitude, and phase functions in Figures 13 and 14 for the 40% span, 10% chord location were typical for the LEX fence-off case at 20 and 32 degrees angle of attack, respectively.

In Figures 13 and 14, the coherence levels are highest in the lower frequencies. Accordingly, the curves for the magnitude and phase are the smoothest at the lower frequencies. Therefore, high coherences indicate high accuracy in the assumed linear input/output relationship between the two signals[15]. The frequency ranges of high coherence exhibited phase angles greater than 100 degrees. This implies that the pressures at a station on the inboard side opposite a station on the outboard side of the tail were not in-phase when tail buffet occurred, resulting in a net differential pressure at that station. This phase relationship would seem to be necessary to account for the net buffet excitation represented by the root bending moment PSDs in Figure 11.

Cross Spectral Densities of the differential pressures at the one station referenced to the differential pressures at another station were also computed. The phase indicated in the cross spectral densities of the differential unsteady pressures between leading-edge and trailing-edge stations offer significant insight into the application of the buffet loads. For instance, if, for some given flight speed, the differential pressures are applied to the tail in a torquing manner (at or near 180 degrees phase between leading-edge and trailing-edge stations), then the participation of the torsion mode in the fatigue of the vertical tail cannot be ignored. However, if this phase relationship is considerably less than 180 degrees, then the participation of the torsion mode in the fatigue of the vertical tail may be less significant.

The phase between the differential pressure at the leading-edge and the diffential pressure at the trailing-edge is shown in Figures 15 and 16. As shown in Figure 15, at 20 degrees angle of attack, the phase around the frequency of the torsion mode at 45 Hz for the full-scale tail is approximately 400 degrees (360 plus 40). This value is far from 180 degrees; however, its significance will be illustrated below when presenting the CSDs for the 1/6-scale test. Similar phase relationships can be extracted from additional CSD plots provided in the reports on the full-scale test[12].

As seen in Figure 16, the phase relationship between the leading-edge and trailing-edge stations at $\alpha = 32^\circ$ in the vicinity of the 45-Hz torsion mode cannot be easily extracted. Typical of the pressure data for the full-scale

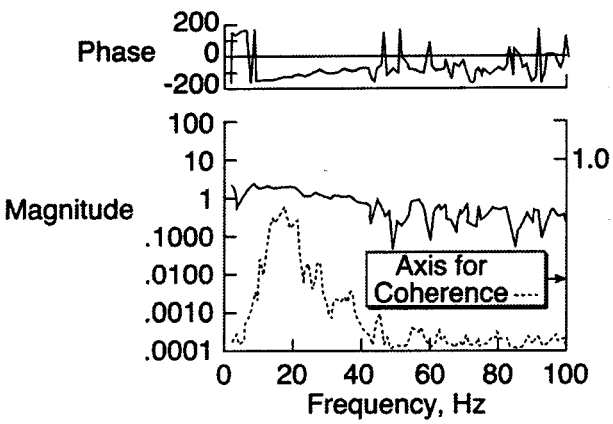

Figure 13. CSD Between Inboard and Outboard Pressures, Full-Scale Tail, $\alpha = 20^\circ$, q = 33 psf, LEX fence off

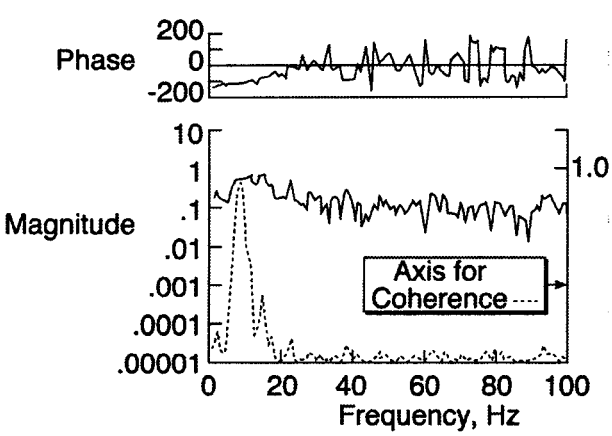

Figure 14. CSD Between Inboard and Outboard Pressures, Full-Scale Tail, $\alpha = 32^\circ$, q = 33 psf, LEX fence off

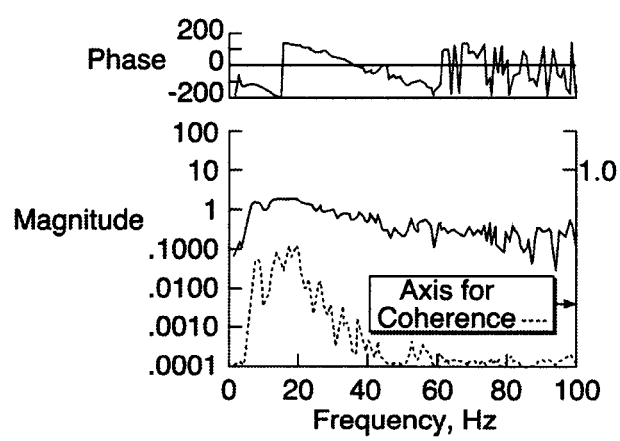

Figure 15. CSD Between Full-Scale Differential Pressures, Stations 1 and 5, $\alpha = 20^\circ$, q = 33 psf, LEX fence off

model at $\alpha = 32^\circ$, these low coherences at the higher frequencies are a result of the low dynamic pressure used in the 80x120 wind-tunnel. In general, by increasing the wind velocity in a tunnel for a given model, the magnitudes of the buffet pressures at the higher frequencies will increase, effectively shifting the peak of the spectra curve to a higher frequency.[3] Therefore, it is difficult, if not impossible, to determine the phase relationship in the vicinity of the torsion mode at the higher angles of attack for the full-scale model.

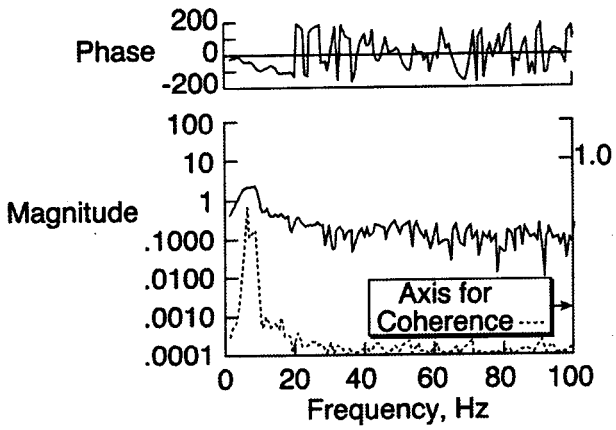

Figure 16. CSD Between Full-Scale Differential Pressures, Stations 1 and 5, $\alpha = 32^\circ$, q = 33 psf, LEX fence off

4.8 1/6-Scale Model Buffet Pressures-Cross Spectral Densities

Cross spectral densities (CSDs) were computed between the unsteady pressures acting on the inboard and outboard surfaces and between the differential unsteady pressures at selected locations on the tail at angles of attack of 20 and 32 degrees. The CSD for the 40% span, 10% chord location at 32 degrees angle of attack is presented as magnitude and phase angle functions in Figure 17 for the flexible tail. Similar to the results shown for the full-scale model in Figure 14, the frequency ranges of high coherence exhibited phase angles greater than 100 degrees. As explained above, this phase relationship would seem to be necessary to account for the net buffet excitation represented by the root strain PSDs in Figure 12.

Cross Spectral Densities of the transducer pair at the leading-edge tip station referenced to the transducer pair at the trailing-edge tip station are shown in Figures 18 and 19 for the flexible tail. At 20 degrees angle of attack, the phase around the frequency of the 1/6-scale tail's torsion mode of 55 Hz is approximately 150 degrees. Therefore, the buffet pressure on the tail is applied in a torquing manner in addition to being applied at the frequency of the torsion mode.

To confirm that the motion of the tail is not producing this phase relationship seen in the pressures of the flexible tail, the same CSDs are plotted for the rigid tail. Comparing the data for the rigid tail in Figure 20 with the data for the flexible tail in Figure 18, the phase values reported on each figure for 55 Hz appear quite similar for 20 degrees angle of attack. Therefore, the response of the tail to the buffet pressures at this angle of attack do not appear to effect the phase relationship around the torsion mode.

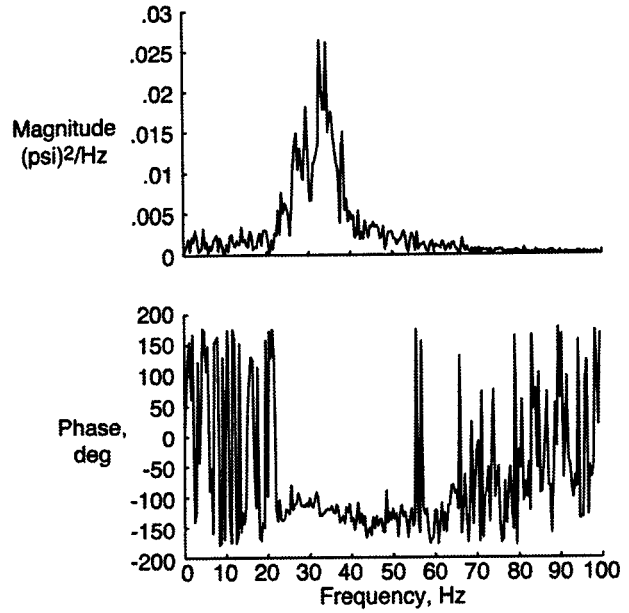

Figure 17. CSD Between Inboard and Outboard Pressures, 1/6-Scale Tail, 40% Span, 20% Chord, $\alpha = 32^\circ$

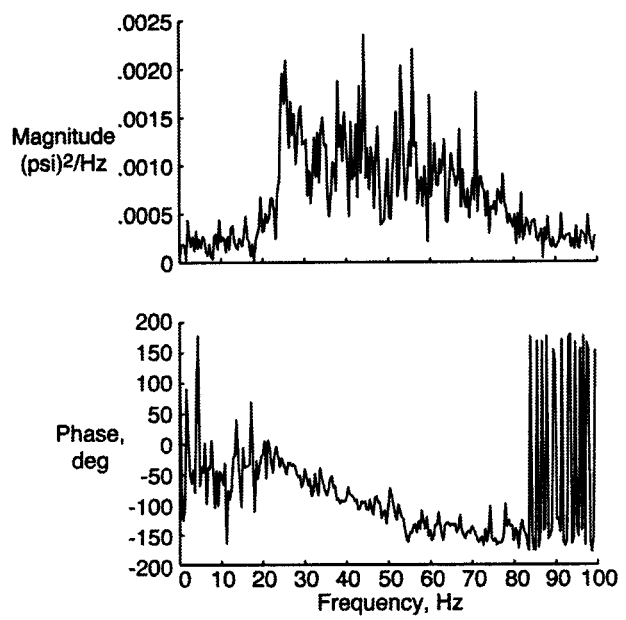

Figure 18. CSD Between 1/6-Scale Differential Pressures, Flexible Tail Stations 1 and 3, $\alpha = 20^\circ$

At an angle of attack of 32 degrees, the phase relationship seen in Figure 19 has changed from the relationship seen in Figure 18 for an angle of attack of 20 degrees. The trajectory of the phase curve between the two stations at 32 degrees angle of attack appears lower than the trajectory of the phase curve at 20 degrees angle of attack, especially when comparing the phase values around 40 Hz on Figures 18 and 19. Although not illustrated but easily

supported by the steady root strains observed during the test, the trajectory of the vortex switched from the outboard side of the tail at the lower angle of-attack to the inboard side of the tail at the higher angle of attack. Vortex position appears to have a direct effect on the phase relationship of the differential pressures between two stations along the vertical tail.

Comparisons of the phase characteristics of the 1/6-scale differential pressures to the full-scale differential pressures shows that a prediction of the full-scale phase can be made from 1/6-scale model data.. From Figure 18, for the 1/6-scale tail, at an angle of attack of 20 degrees, the phase at the frequency of the torsion mode of 45 Hz for the full-scale tail is approximately 100 degrees. Again, from Figure 15, the phase measured on the full-scale tail at 45 Hz is approximately 400 degrees.

A scale factor between the phase of the 1/6-scale CSDs and the phase of full-scale CSDs can be derived from a relationship between angular velocity and time. Shown in Equation (4a), angular velocity can be converted to frequency, and time, t, may be obtained by dividing the distance, d, between two transducer stations by the velocity, v, of the freestream flow. The scale factor, shown in Equation (4b), is obtained by dividing the results of Equation (4a) for the 1/6-scale model by the results of Equation (4a) for the full-scale (aircraft) model.

$$\phi = \omega t = (2\pi f)\cdot\left(d/v\right) \qquad (4a)$$

$$\left(\frac{\phi_{model}}{\phi_{aircraft}}\right) = \frac{f_m d_m v_a}{f_a d_a v_m} = 0.255 \qquad (4b)$$

Using data presented earlier for both models and wind-tunnel conditions, the phase scale factor between the 1/6-scale and full-scale tails, for a frequency ratio of one, is 0.255. The ratio of the two values of phase stated above for 45 Hz is 0.25.

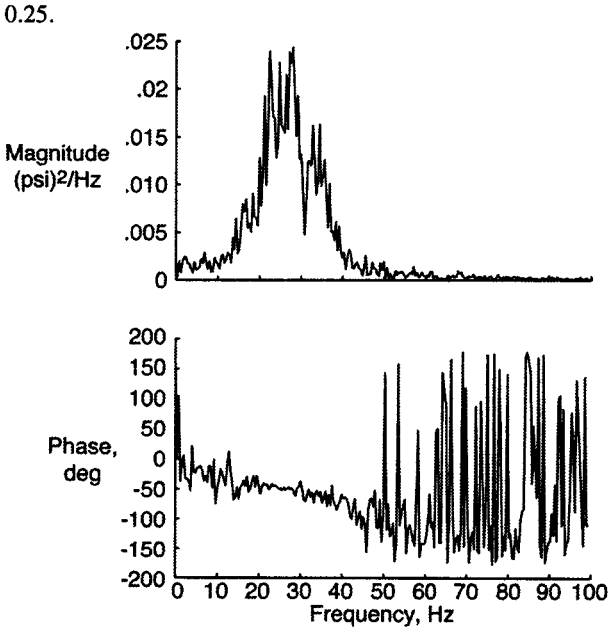

Figure 19. CSD Between 1/6-Scale Differential Pressures, Flexible Tail Stations 1 and 3, $\alpha = 32^\circ$

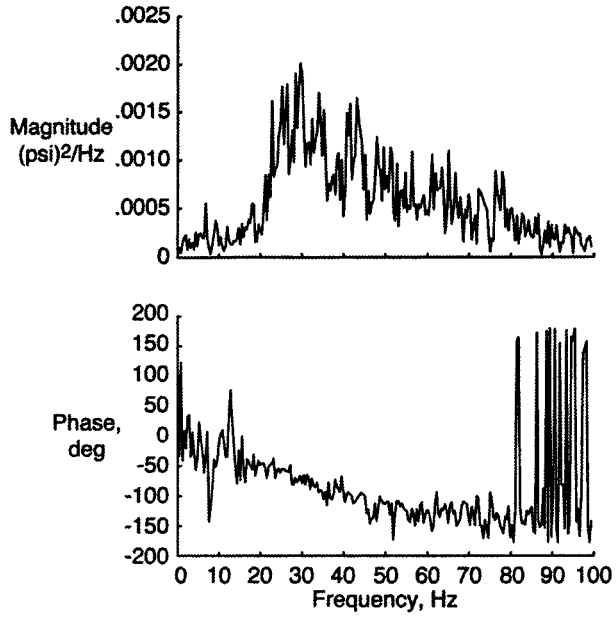

Figure 20. CSD Between 1/6-Scale Differential Pressures, Rigid Tail Stations 1 and 3, $\alpha = 20^\circ$

Comparisons were made for the phase of the differential pressures at other stations on the full-scale and 1/6-scale with similar results. Rough estimates of the phase relationship for any two stations on the full-scale tail can be extracted from the CSDs of the 1/6-scale tail using equation (4). In addition, by using equation (4), one may predict the phase of the differential pressures at the frequency of any tail mode for other flight conditions. Since the first bending and first torsion mode are the only two modes that affect the fatigue life of the vertical tails on the F/A-18, the phase relationships of interest would be at the frequencies associated with these two modes.

Because the dynamic pressure used for the 1/6-scale model is the (scaled) equivalent of 340 psf for the full-scale aircraft, the magnitudes of the buffet pressure are higher at the higher frequencies for the higher angles of attack than seen in the full-scale data[1, 12]. This is confirmed by comparing the data in Figures 14 and 19. In Figure 19 for the 1/6-scale model at 32 degrees angles of attack, the phase at 40 Hz is well below 100 degrees. Therefore, the buffet pressures are not being applied to the tail in a torquing manner at the higher angles of attack.

The loss in response of the tail in its torsion mode around 58 Hz at the higher angle of attack, as seen by comparing Figures 12(a) and 12(b), confirm two aspects of the buffet pressures at the higher angles of attack: 1) the buffet pressures are no longer being applied to the tail as a torque; and 2) the magnitudes of the buffet pressures around 58 Hz are significantly lower at the higher angles of attack than the magnitudes associated with the lower angles of attack.

The effects of the response of the flexible tail to the buffet in the first bending mode around 16 Hz can be seen in the magnitude and phase plotted in Figure 19. To confirm this, the CSD between the same two stations on the rigid tail

at the same conditions are provided in Figure 21. In Figure 21, the magnitude and phase around 16 Hz for the rigid tail is not as pronounced as shown in Figure 19 for the flexible tail.

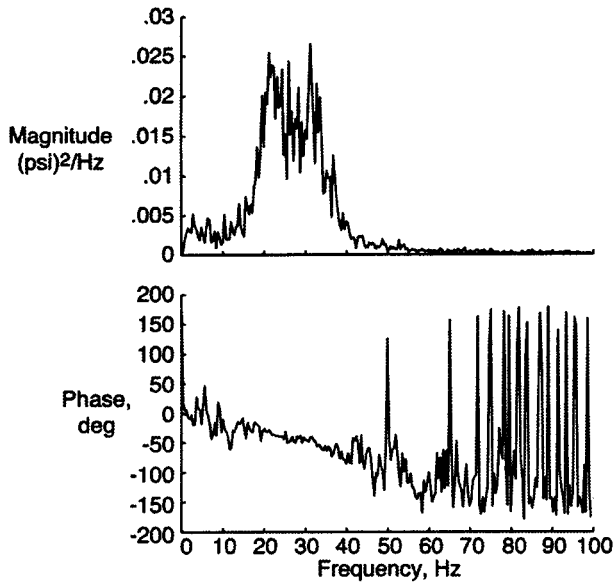

Figure 21. CSD Between 1/6-Scale Differential Pressures, Rigid Tail Stations 1 and 3, $\alpha = 32^\circ$

5. Concluding Remarks

Full-scale wind tunnel tests were conducted to quantify the pressures responsible for inducing tail buffet on the F/A-18. The resulting tail-tip accelerations were also measured. The LEX fence was shown to effectively reduce the RMS root bending moments, as well as the corresponding spectral levels, up to 32 degrees angle of attack at zero sideslip. Higher angles-of-attack reduced the benefits of the LEX fence. Higher angles-of-attack caused the buffet pressures to be concentrated in a narrow, low frequency band. Dynamic pressure scale effects on the RMS root bending moment were found to be minimal under the current test conditions.

For the full-scale model, cross-spectral densities between the buffet pressures on the inside and outside surfaces of the starboard tail showed strong coherence and phase relationships at the lower angles of attack.

Wind tunnel tests of a 1/6-scale F/A-18 model were conducted at the Transonic Dynamics Tunnel to determine, among other aspects, the phase relationship of the unsteady pressures on the outboard and inboard surfaces (as well as differential) of flexible and rigid vertical tails on both sides of the model.

Comparison of the 1/6-scale data to the full-scale data reveal similarities in the trends of the spectral content as a function of angle of attack. The phase between inboard and outboard transducers at one station was nearly identical for both models. The phase of the differential unsteady pressures between two stations on the 1/6-scale model may be scaled up to identically located stations on the full-scale vertical tail using the scaling relationship in equation (4). Equation (4) may also be used to predict the phase of the differential pressures at the frequency of any tail mode for other flight conditions.

6. Acknowledgements

The authors wish to acknowledge the cooperation of the NASA Ames and the NASA LaRC F/A-18 Wind Tunnel Test Teams especially. The authors also wish to acknowledge the technical advice provided by Dr. Holt Ashley of RANN Corporation and Dr. Marty Ferman, formerly of McDonnell Douglas Corporation.

7. References

1. Pettit, C. L., Brown, D. L., and Pendleton, E., "Wind Tunnel Tests of Full-Scale F/A-18 Twin Tail Buffet: A Summary of Pressure and Response Measurements," AIAA-94-3476, proceedings of the AIAA Atmospheric Flight Mechanics Conference, Scottsdale, AZ, August 1994.
2. Lee, B. H. K., Brown, D., Zgela, M., and Poirel, D., "Wind Tunnel Investigation and Flight Tests of Tail Buffet on the CF-18 Aircraft," in Aircraft Dynamic Loads Due to Flow Separation, AGARD-CP-483, NATO Advisory Group for Aerospace Research and Development, Sorrento, Italy, April 1990.
3. Zimmerman, N.H. and Ferman, M.A., "Prediction of Tail Buffet Loads for Design Application," NADC-88043-60, July 1987.
4. Shah, G.H., "Wind-Tunnel Investigation of Aerodynamic and Tail Buffet Characteristics of Leading-Edge Extension Modifications to the F/A-18," AIAA Paper 91-2889, August 1991.
5. Meyn, L.A. and James, K.D., "Full Scale Wind Tunnel Studies of F/A-18 Tail Buffet," AIAA Paper 93-3519, August 1993.
6. Lee, B.H.K. and Brown, D., "Wind-Tunnel Studies of F/A-18 Tail Buffet," Journal of Aircraft, Vol. 29, No. 1, Jan.-Feb. 1992.
7. Lee, B.H.K. and Tang, F.C., "Buffet Load Measurements on an F/A-18 Vertical Fin at High-Angle-of-Attack," AIAA-92-2127-CP.
8. Lee, B.H.K., Brown, D., Tang, F.C., and Plosenski, M., "Flowfield in the Vicinity of an F/A-18 Vertical Fin at High Angles of Attack," Journal of Aircraft, Vol. 30, No. 1, Jan.-Feb. 1993.
9. Lee, B.H.K. and Tang, F.C., "Unsteady Pressure and Load Measurements on an F/A-18 Vertical Fin," Journal of Aircraft, Vol. 30, No. 5, Sept.-Oct. 1993.
10. Rizk, Y.M. and Gee, K., "Numerical Prediction of the Unsteady Flowfield around the F-18 Aircraft at Large Incidence," AIAA Paper 91-0020, January, 1991.
11. Ferman, M.A., Patel, S.R., Zimmerman, N.H., and Gerstenkorn, G., "A Unified Approach to Buffet Response of Fighter Aircraft Empennage," from Aircraft Dynamic Loads due to Flow Separation, AGARD-CP-483, 1990.
12. Pettit, C.L., Banford, M., Brown, D., and Pendleton, E., "Pressure Measurements on an F/A-18 Twin

Vertical Tail in Buffeting Flow," Volume 1-4, WL-TM-94-3039, August 1994.

13. Levraea, V.J., Henderson, D.A., Pacia, A.P., and Banford, M.P., "Modal Survey of a Full-Scale F-18 Wind Tunnel Model," WL-TM-92-350-FIBG, September 1992.
14. Mabey, D.G., "Some Aspects of Aircraft Dynamic Loads due to Flow Separation," AGARD-R-750, 1987.
15. Bendat, J. S., and Piersol, A. G., Random Data, Wiley-Interscience, New York, 1986.

REPORT DOCUMENTATION PAGE

Form Approved
OMB No. 0704-0188

Public reporting burden for this collection of information is estimated to average 1 hour per response, including the time for reviewing instructions, searching existing data sources, gathering and maintaining the data needed, and completing and reviewing the collection of information. Send comments regarding this burden estimate or any other aspect of this collection of information, including suggestions for reducing this burden, to Washington Headquarters Services, Directorate for Information Operations and Reports, 1215 Jefferson Davis Highway, Suite 1204, Arlington, VA 22202-4302, and to the Office of Management and Budget, Paperwork Reduction Project (0704-0188), Washington, DC 20503.

1. AGENCY USE ONLY *(Leave blank)*

2. REPORT DATE
August 1996

3. REPORT TYPE AND DATES COVERED
Technical Memorandum

4. TITLE AND SUBTITLE
A Comparison of Pressure Measurements Between a Full-Scale and a 1/6-Scale F/A-18 Twin Tail During Buffet

5. FUNDING NUMBERS
WU 505-63-50-13

6. AUTHOR(S)
Robert W. Moses and Ed Pendleton

7. PERFORMING ORGANIZATION NAME(S) AND ADDRESS(ES)
NASA Langley Research Center
Hampton, VA 23681-0001

8. PERFORMING ORGANIZATION REPORT NUMBER

9. SPONSORING / MONITORING AGENCY NAME(S) AND ADDRESS(ES)
National Aeronautics and Space Administration
Washington, DC 20546-0001

10. SPONSORING / MONITORING AGENCY REPORT NUMBER
NASA TM-110282

11. SUPPLEMENTARY NOTES

12a. DISTRIBUTION / AVAILABILITY STATEMENT
Unclassified—Unlimited

Subject Category 05

12b. DISTRIBUTION CODE

13. ABSTRACT *(Maximum 200 words)*

In 1993, tail buffet tests were performed on a full-scale, production model F/A-18 in the 80- by 120-Foot Wind Tunnel at NASA Ames Research Center. Steady and unsteady pressures were recorded on both sides of the starboard vertical tail for an angle-of-attack range of 20 to 40 degrees and at a sideslip range of -16 to 16 degrees at freestream velocities up to 100 knots (Mach 0.15, Reynolds number $1.23*10^7$). The aircraft was equipped with removable leading edge extension (LEX) fences that are used in flight to reduce tail buffet loads.

In 1995, tail buffet tests were performed on a 1/6-scale F-18 A/B model in the Transonic Dynamics Tunnel (TDT) at NASA Langley Research Center. Steady and unsteady pressures were recorded on both sides of both vertical tails for an angle-of-attack range of 7 to 37 degrees at freestream velocities up to 65 knots (Mach 0.10).

Comparisons of steady and unsteady pressures and root bending moments are presented for these wind-tunnel models for selected test cases. Representative pressure and root bending moment power spectra are also discussed, as are selected pressure cross-spectral densities.

14. SUBJECT TERMS
Tail buffet, pressure measurements, tail buffeting

15. NUMBER OF PAGES
13

16. PRICE CODE
A03

17. SECURITY CLASSIFICATION OF REPORT
Unclassified

18. SECURITY CLASSIFICATION OF THIS PAGE
Unclassified

19. SECURITY CLASSIFICATION OF ABSTRACT
Unclassified

20. LIMITATION OF ABSTRACT